Glass Europe Vol. 3 (2025) 239-251
https://doi.org/10.52825/glass-europe.v3i.2569

Submitted: 26 Dec. 2024 | Accepted: 10 Sep. 2025 | Published: 05 Dec. 2025

Long-Range Transformations During Crystallization in Solid and Softening Glass

Elena A. Chechetkina*

Institute of General and Inorganic Chemistry of Russian Academy of Sciences (1980-2011), Moscow, Russia

*Correspondence: Elena A. Chechetkina, eche2010@yandex.ru

Abstract. The glassy state is considered as a result of self-organization in the form of the bond wave which stipulates a hierarchical structure up to the non-crystalline long-range order characterized by the bond wave length and the wave direction. The model is tested using original experiment of the cavitation-assisted crystallization with a special attention to the pre-nucleation stages observed by means of IR-spectroscopy and SEM. As a result, a three-step model for crystallization in glass is proposed based on the macroscopically extended 2D wavefronts as nuclei. The model is compared with classical nucleation theory and contemporary trends in glass science concerning intrinsic heterogeneity, both structural and dynamical.

Keywords: Glass, Self-Organization, Crystallization, Nucleation, Pre-Nucleation Phenomena, Non-Crystalline Long-Range Order, Cavitation Treatment

1. Introduction

Despite of intensive debates about the nature of the glassy state for at least a century, glass remains an enigmatic material up to now. The main topics are glass structure, glass transition and crystallization in glass and glass-forming liquids [1]. Nevertheless, it is still unclear even why glass-forming melts can be supercooled far below melting points without crystallization up to formation of bulk non-crystalline solid named glass. A common explanation appeals to classical nucleation theory (CNT) and the barrier approach with high enough barriers of nucleation and growth $G',G''>30RT_m$ as the condition for glass formation [2]. Another approach, which is also based on CNT, is the T-T-T (time-temperature-transformation) diagram used for calculation of critical cooling rate for a chosen degree of crystallinity [3].

The crystallization experiment, however, reveals a significant deviation from CNT. The most confusing point is an enormously long *lag time* before nucleation [4], a fact that is interpreted by the authors as 'a hit to metastable polymorphs at the nanoscale'. However, these “polymorphs”, even being very small, are just crystalline formations. In contrast, the non-crystalline “initial reorientation” (IRO) stage, after which crystallization can begin, was introduced by us in 1981 [5]. Unfortunately, the IRO was not proved experimentally so far.

The CNT inability to describe crystallization data is probably due to the assumed *homogeneity* of glass structure which corresponds to classical *continuous random network* (CRN) model after Zachariasen [6]. Contemporary development of the CRN model in frames of the *topological constraint theory* [7] cannot eliminate this cause since the network remains homogeneous even when a special “*intermediate phase*” appears within a definite composition range corresponding to a favorable arrangement of covalent bonds. Attribution of “intermediate phase” to the self-organized state [8] not only eliminate the network homogeneity but also

discredits the term “self-organization”, which has become so widely used that it risks losing its meaning.

Here I propose to return to the classical notions about self-organization [9], [10], which I previously applied to the glassy state by means of the *bond wave* model [11]. The *bond wave* is considered as the *dissipative pattern* that realizes in every glass irrespectively of its chemical composition, in contrast to “intermediate phase” which occurs only within a definite composition range. The second difference is the introduction of an alternative bonding state - *alternative bond* - which is inclined to collective behavior in the form of spatiotemporal correlation between bond-exchange events. The substances whose chemical-bonding system ensure such a behavior can form glass and acquires a set of specific properties, some of which (viscosity, fracture, first sharp diffraction peak) was considered by me earlier (see [12], [13] for a brief review). In this article the bond wave model is applied to crystallization with the use of our previous experiments on cavitation treatment of softening selenide glasses [14], [15]. As a result, the non-classical three-stage model for crystallization is formulated, whose main point is the extended 2D “nuclei” in the form of the bond wave wavefront. Despite of unusual character, the model correlates with contemporary glass theory and provides practical recommendations.

2. Model

Glass is considered commonly as “amorphous” material having no *long-range order* (LRO) “by definition”. This definition, however, is not more than a statement “glass is not a crystal”. Really, a series of sharp peaks observed in diffraction pattern of crystal is absent in glass, where the only one relatively sharp peak is observed at Q_1~1cm^{-1}. This First Sharp Diffraction Peak (FSDP), however, disappears in radial distribution function, a standard method for describing glass structure which is therefore considered as “amorphous” a *priori*. The FSDP has payed attention only in the middle of 20th century as a signature of the so-called *medium-range order* (MRO) on the **d**=2π/Q_1~6Å scale, a very popular theme now. Two main models of FSDP/MRO have been proposed: the *layer* model after Vaipolin & Porai-Koshits [16] and the *void* model proposed by Elliott [17]. Both, however, have limitations [18]; the first one because far from all glasses have the layer-type crystalline counterpart, the second one because the “cation-centered” voids need a related chemical composition. Both models cannot explain why FSDP is so sharp.

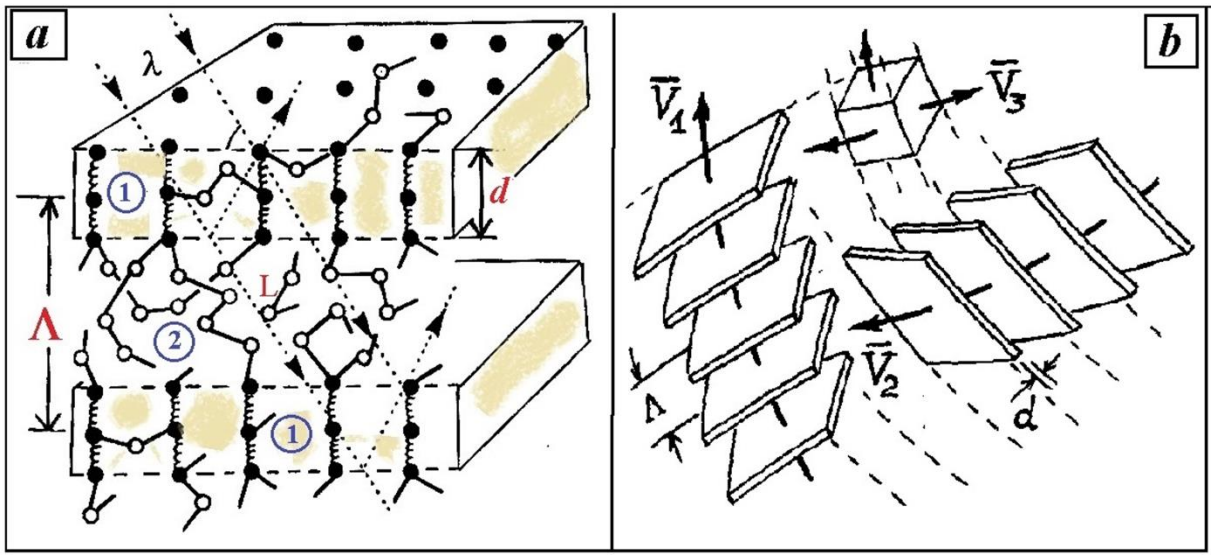

Figure 1. *(a) The bond wave elementary cell containing two wavefronts ‘1’ and CRN ‘2’ between them; (b) The soliton-like Intersection of three bond waves.*

Being based on the bond wave model [19], I have proposed the *modified model of FSDP* [20] which considers FSDP as a collective reflection from equidistant layers of the **d** thickness shown in Fig.1a. The layers are themselves part of a *hierarchical structure* denoted as SRO(**L**)↔MRO(**d**)↔LRO(**Λ**), where **L** is the basic bond length, **d** is the wavefront thickness and **Λ** is the wavelength.

To form the bond wave, a substance needs two properties: (*i*) the two-state bonding, when the basic bond (usually two-center two-electron covalent bond, CB) can transfer reversibly into a higher-energy alternative bond, AB, and (*ii*) the spatiotemporal correlation between elementary acts of bond exchange, ΣΣ(CB↔AB). The first condition was justified by Dembovsky, initially in the form of "quasi-molecular defects" [21], representing three-center four-electron bonds imbedded in covalent network (these 3c-4e bonds are shown by springs in Fig. 1a), and then in a general form of hypervalent bonds [22]. The second condition was studying by me since 1991 [19] until now by searching of the bond wave marks in real experiments [12], [13].

The general experiment concerns the phenomenon of glass transition, which is considered as the *dimensionality* transition of the refrozen bond wave state, 3D→2D. Above T_g the 3D bond wave animates all the structure, thus providing related properties, viscosity first. Below T_g only 2D bond waves represented by collective strings moving along the stopped layers, which correspond to the wavefronts of the previously frozen 3D bond wave. These layers give a collective reflection of the probing X-ray beam (see λ in Fig. 1a) in the form of FSDP observed at $Q_1=2\pi/\mathbf{d}$, where **d** in the layer/wavefront thickness. The *sharpness* of FSDP is a consequence of the bond wave itself. However, to observe the bond wave reflection at $Q_{\Lambda}=2\pi/\mathbf{\Lambda}<<Q_1$ (e.g., at $0.06 Å^{-1}$ for **Λ**=100Å) one should investigate the low-Q region by means of a special equipment like synchrotron.

The frozen wavefronts can be observed through fracture which develops along the layers populated with relatively weak alternative bonds. The observed fractures [12], [13], [23] indicates the *solitonic* behavior of the bond wave which allows waves to intersect without distortion, thus creating layer, columnar, or cellular substructure corresponding to one, two or three intersecting bond waves, as it is shown in Fig. 1b. The waves direction is given by one, two or three *information fields* [12], [13] respectively.

Based on these previous remarks, one can propose the following picture for crystallization. First, the process begins on the wavefronts enriched by the high-energy alternative bonds - the energy difference between common covalent bond (ground state) and alternative bond (excited state) was evaluated by quantum-chemical modelling of typical glass-formers by Dembovsky et al. (see review [22] and references therein). Alternative bonds can switch covalent bonds from some atoms to others [21]; the collective switching needed for macroscopic processes like viscous flow [13] and crystallization proceeds not only within the wavefronts by means of 2D bond waves but also in the whole network by means of 3D bond waves at $T>T_g$. Thus, in solid glass ($T<T_g$), crystallization begins on the stopped wavefronts and then spreads into the covalent surrounding (Fig. 2a,b). When crystallization begins at $T>T_g$, nucleating agents are needed, e.g., suitable impurities, to interact with the moving wavefronts and distort them, as shown in Fig. 2c. Here the wavefront energy dissipates also into crystallization around the impurity, and the bond wave becomes weaker, up to its complete disappearance when the crystalline-type long-range order wins. Finally, in Fig. 2d there is a scheme of cavitation treatment of softening glass with ultrasonic (US) information field to give the 3D bond wave direction.

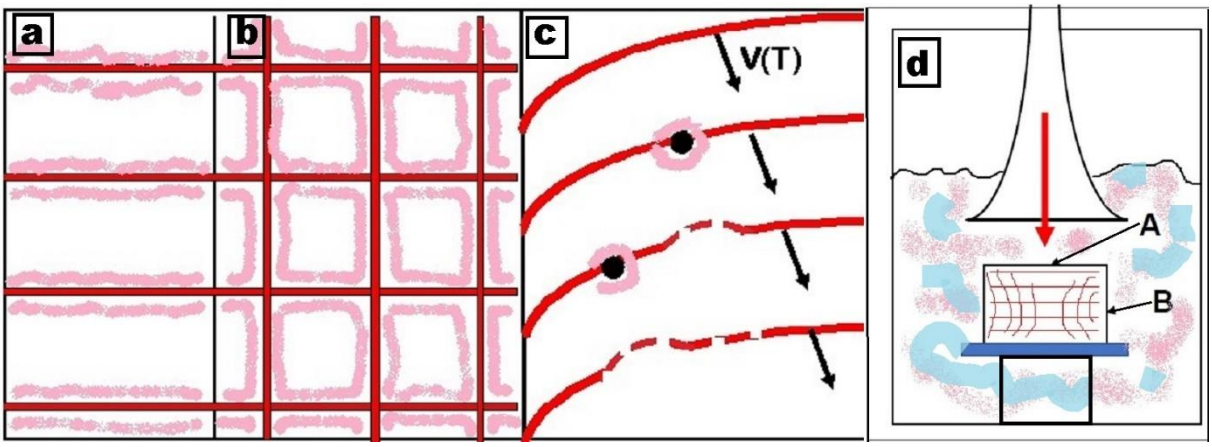

Figure 2. *Model for crystallization in (a) solid glass containing one bond wave, (b) solid glass with two bond waves; (c) supercooled liquid. Scheme of cavitation experiment (d), where thick red arrow is the US input and thin lines/curves in the sample are the section of the wavefront families.*

3. Experiment

3.1. Samples: Composition and History

Selenium was chosen as the model substance because, besides being an elementary glass-former, its glass transition temperature T_g(Se) ≈ 35ºC is low enough to use water as the cavitation medium. Four elements (Te, S, As, Cl) were added to Se to investigate the impurity effect on kinetics and morphology of crystallization. Corresponding four Se-X series, each containing 5-6 samples from 0 %X to 10% for X=Te or S, 5% for As and 0.3% for Cl (at%), were prepared five years before this study in the form of tablets of 25 mm diameter and **d***=15 mm thickness. The samples investigated immediately by ultrasound velocity and X-ray absorption have demonstrated a strong ***non-linearity*** on the concentration-property curves at 1-2% for Te/S, at 0.5-1% for As and at 0.01-0.05% for Cl (see Fig. 5 in [24]). The *transparency* **T***, which is measured by optical transmission at 1000 cm^{-1}, was practically the same for all the samples (**T*** = 66 ± 2 %, a value typical for good selenide glasses of the same 15 mm thickness). However, it began to decrease in different way depending on composition after ageing/relaxation and special treatments indicated in Table 1. All samples of a given series have the same history, which was varied from series to series during this study.

Table 1*. History of the Se-Te series and related change of transparency for pure Se (0% Te).*

Step	Sign	τ, mth	Δτ, mth	d*, mm	T*(A), %	T*(B), %	Comment
1	F	0	0	15	68	-	Fresh sample
2	R1	60	60	14	39.12	-	Relaxation
3	S1	62	2	13	66.55	-	Surface resection
4	S2	70	8	12	56.26	64.18	From tablet to block
5	U1	71.5	1.5	12	1.71	2.45	40°C, 5 min
6	R2	80.5	9	12	2.16	3.10	Relaxation
7	U2	82.5	2	12	1.25	3.86	50°C, 3 min
8	S3	83.5	1	11	54.76	63.60	Surface resection
9	U3	83.5	0	11	54.65	65.12	40°C, 5 min
10	U4	83.5	0	11	52.34	59.56	50°C, 5 min
11	R3	123.5	40	11	36.15	no data	Relaxation
12	U5	123.5	0	11	4.18	13.81	72°C, 2 min
13	SEM1	124.5	1	-	-	-	Figs. 7a, b
14	SEM2	127	2.5	-	-	-	Fig. 7c

The steps are: R - relaxation at room temperature for $\Delta\tau$ months (mth), S - surface resection by mechanical removing 0.5 mm from each grain, U - cavitation treatment. After each step the samples were measured by optical transmission as soon as possible. The step succession is defined by the experimental logic. For example, step S2, performed before the first US-treatment (U1), prepares the samples for the study of the cavitation-induced anisotropy by formation of lateral B-grains (see A and B in Fig. 2d) of the same **d***. A gradual increase of the cavitation treatment temperature, from 40ºC for U1 to 72ºC for U5, prevents fast reduction of sample transparency. Some of final samples were split in different directions (A or B) to investigate their internal structure by electron microscopy (steps 13 and 14).

3.2. Results: The optical transmission spectra

The experiment was controlled by optical transmission spectra measured in the region of 350-5000 cm^{-1} subdivided in "vibrational spectrum" below 1000 cm^{-1} (Fig. 3a) and "transparency window" above (Fig. 3b). The 490 cm^{-1} and 740 cm^{-1} absorption bands correspond to the 2nd and 3rd overtones of main Se band located at 245 cm^{-1} [25]. The transparency window is applied commonly for detection of impurities which manifest themselves by characteristic bands [26]. Usual uncontrolled contaminations like hydroxyl, water or carbon [27] are absent in our samples; weak tips observed at ω>1000 cm^{-1} (see Figs. 3 and 5 below) are of another origin.

Fig. 3 corresponds to *spontaneous* crystallization after 5-years ageing. Note that here and below the term "crystallization" is used in a wide sense, including pre-nucleation stage.

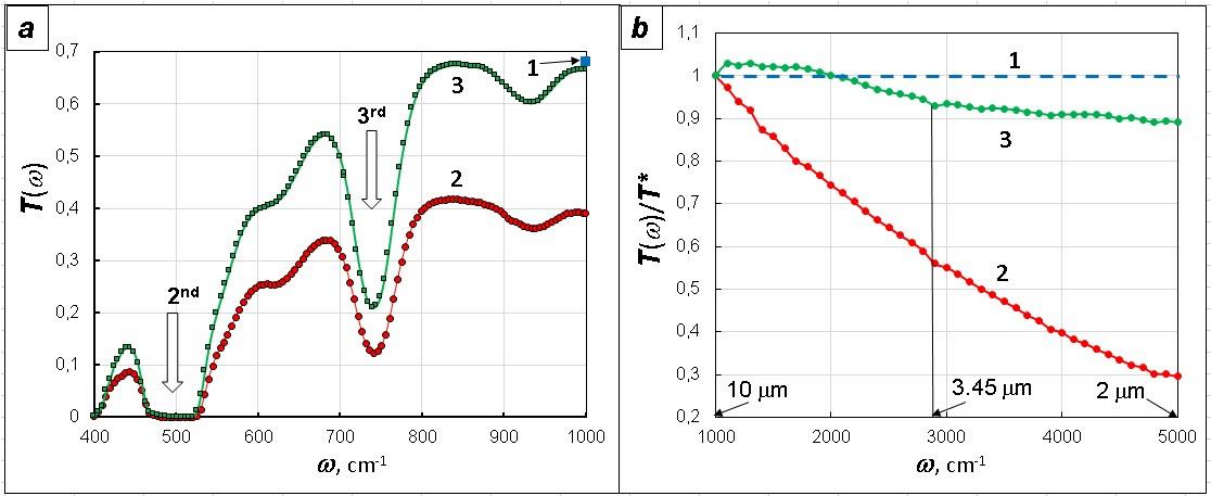

Figure 3. *The ageing of Se glass as reflected in (a) vibrational spectrum and (b) transparency window. Notations: 1 - fresh sample, 2 - aged sample, 3 - aged sample after surface resection.*

As shown in Fig. 3a, the form of *vibrational spectra* of the aged Se sample is the same ('2' and '3'), but the form in the *window of transparency* in Fig. 3b changes very strongly. This means there is no change in short-range order, but the higher-order formations appear that behave as the scattering objects (ScO). These ScO are responsible for both reduction of transparency, **T***=**T**(1000 cm^{-1}), and change of the window form T(ω)/T* at ω>1000 cm^{-1}. The fact that both are restored after removing of the surface layer of the 0.5 mm thickness (2→3) points to the *surface* location of these ScO in Se. Other Se-Te samples, however, demonstrate a more complex surface/volume distribution of ScO developing at ageing. To characterize this distribution, let us introduce the ***extent of heterogeneity*** in the form of

$$G = (T^*_3 - T^*_2) / (T^*_1 - T^*_2) \quad (1)$$

As shown in Fig. 4a, the samples of Se-Te series behave in a strongly *non-linear* way, when almost completely heterogeneous Se ($\mathbf{T^*_3 \approx T^*_1}$) becomes almost completely homogeneous ($\mathbf{T^*_3 \approx T^*_2}$) when adding only 2%Te, and then return to a monotonous behavior, which is expected from a simple fish-like form of the Se-Te equilibrium phase diagram.

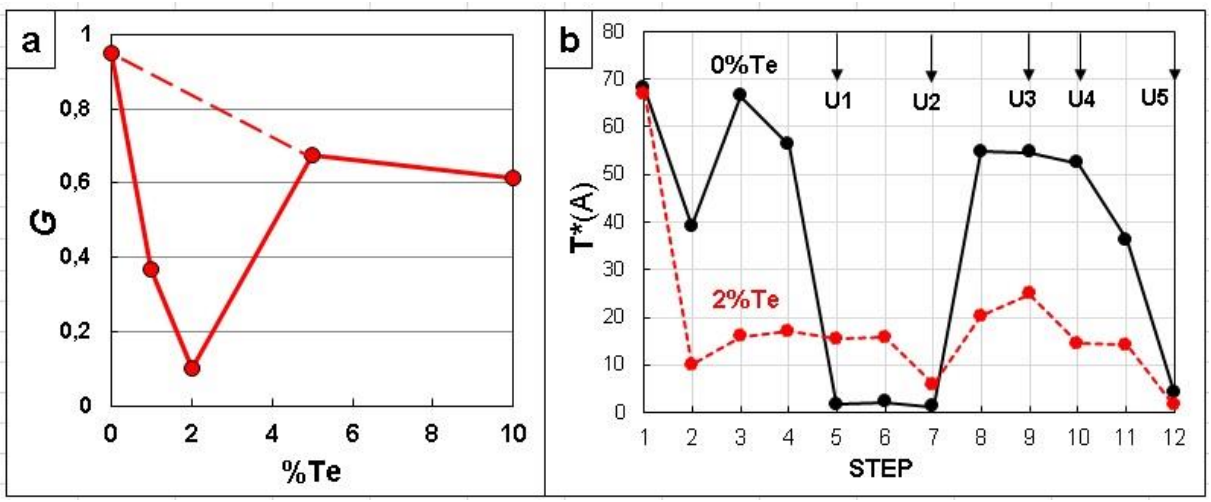

Figure 4. *(a) Optical heterogeneity* ***G*** *by Eq.(1) for the aged samples of Se-Te series; (b) Transparency change during experiment for Se (solid black lines) and Se-2%Te (dotted red lines) samples.*

The difference between “normal” Se and “extremal” Se-2%Te samples remains throughout the subsequent experimental steps, as it is shown by the transparency data in Fig. 4b. The most remarkable effect occurs during the first cavitation treatment (U1, 40ºC) which darkens the 0%Te sample almost completely (56%→2%) but there is practically no influence on the 2%Te sample (17%→15%). In contrast, the repeated treatment at the same temperature (U3, 40ºC) does not influence the restored 0%Te sample, but it increases the 2%Te sample transparency (20%→25%), a result that can be considered as the cavitation-induced resolving of the previously formed ScO. The last cavitation treatment at 72ºC (U5) generates scattering objects in both samples so intensively that the difference between them practically disappears, at least in terms of transparency.

A high sensitivity of our digital spectrometer permits to search fine effects even in the samples of a low transparency such as those shown in Fig. 5. The main effects observed in the window of transparency region are: (*i*) development of optical *anisotropy*, (*ii*) change of the window *form* and (*iii*) change of *heterogeneity*. Optical anisotropy, **T**(A)≠**T**(B), which is small but clear after first 50ºC cavitation treatment (compare spectra 7 in Fig. 5a), becomes very large after the 72º treatment (compare spectra 12 in Fig. 5b). The form of both ‘7’ and ‘12’ spectra is obviously different, bending in different directions for 7A, 7B, 12B and 12 A which demonstrates especially rapid fall of transmission with frequency. This behavior results in maximum anisotropy around 2000 cm^{-1}. Note that the sign of anisotropy changes: **T**(A)>**T**(B) for U2 in Fig. 5a *versus* **T**(A)<**T**(B) for U5 in Fig. 5b.

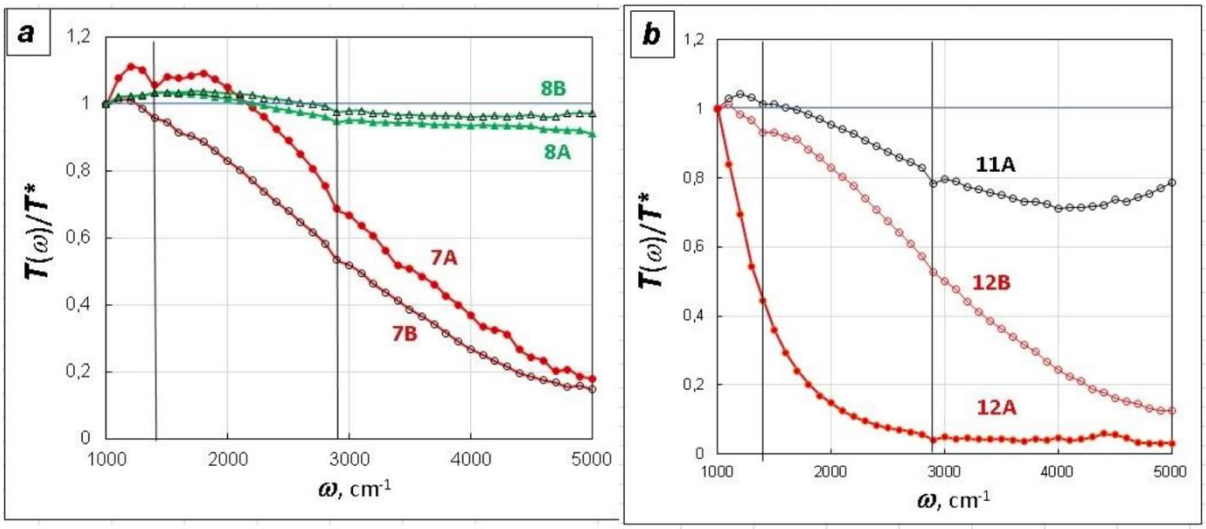

Figure 5. *The optical transmission spectra of pure Se (0%Te) measured in frontal (A) and lateral (B) directions. (a) after the second US-treatment (U2 at 50ºC, step 7) and the surface resection (step 8); (b) before the final US-treatment (step 11) and after it (U5 at 72ºC, step 12)*

Regarding the extent of heterogeneity, the restoration of the constant-transmission form for spectra 8A and 8B (compare with spectra 3 in Fig. 3b) indicates that heterogeneous distribution of the developing ScO persists (compare with G=0.95 for Se in Fig. 4a). Unfortunately, a direct estimation of heterogeneity for the U5 case is impossible because of a critical thinning of Se sample when using the applied 9 mm aperture (**d***=11 mm for the final samples - see Table 1). Therefore, one cannot conclude surely where the final ScO are located. However, unusual form of the previous spectra 11A, which was obtained after U3 and U4 treatments and the following relaxation R3 (see Fig. 4b for 0%Te), permits to propose that the prior U3 and U4 treatments have activated Se sample in such a way that ScO generated during 40-months relaxation (R3) have developed both in the surface and the volume of the sample.

To conclude this subsection, let note weak tips observed at 1000, 1400 and 2900 cm^{-1} which can be associated with the scattering objects of dimensions 10, 7.1 and 3.45 μm, respectively. To understand the nature of these objects, their real size and morphology, one should add other experimental methods, scanning electron microscopy (SEM) first.

3.3. Results: Fractures observed by SEM

The final samples have demonstrated various forms - from very similar to initial rounded blocks to crumpled or even partially fractured samples - depending on the Se-X series and concentration of the X addition. For example, the Se-S series consisting of six samples from 0.25%S to 10%S is shown in Fig.6. The initial 0%S sample is absent here because it coincides with the 0%Te sample since Se-Te and Se-S series were prepared under identical conditions. Note also that 0.25%S sample is presented by a half of the rounded block because it was cracked at the preceding resection of surface layer. The crumpled exterior, most expressed for the 2-10%S compositions, could be explained by the low glass transition temperature of sulfur T_g(S)=−25ºC unless the fact that simple additivity gives T_g^{add}(2%S)=34ºC and T_g^{add}(10%S)=29ºC , i.e. only for 1-6 degrees below T_g=35ºC for pure Se. This is one more indication of the non-linear reaction of Se matrix on incorporation of foreign atoms.

Figure 6. *The samples of the Se-S series from the frontal (top) and lateral (bottom) view after the final cavitation treatment of 72ºC.*

Despite of a rather different exterior, all final samples looked like glass rather than a crystal. The *fractures*, made along A and B grains, also looked "glassy" (bright and smooth) when observed by the naked eye. The SEM picture, however, gives a more complex picture. For example, A-fracture of pure Se in Fig. 7a (step 13 in Table 1) looks like a carpet of the crystal-like needles of ~1 μm size, while B-fracture demonstrated a uniform field (Fig. 7b) usual for glass. The repeat observation after 2.5 months (step 14) showed the same image for A-fracture, but the appearance of clews of "spiders" on the B-fracture (Fig. 7c). Note that all the fractures were made *just before* the SEM examination.

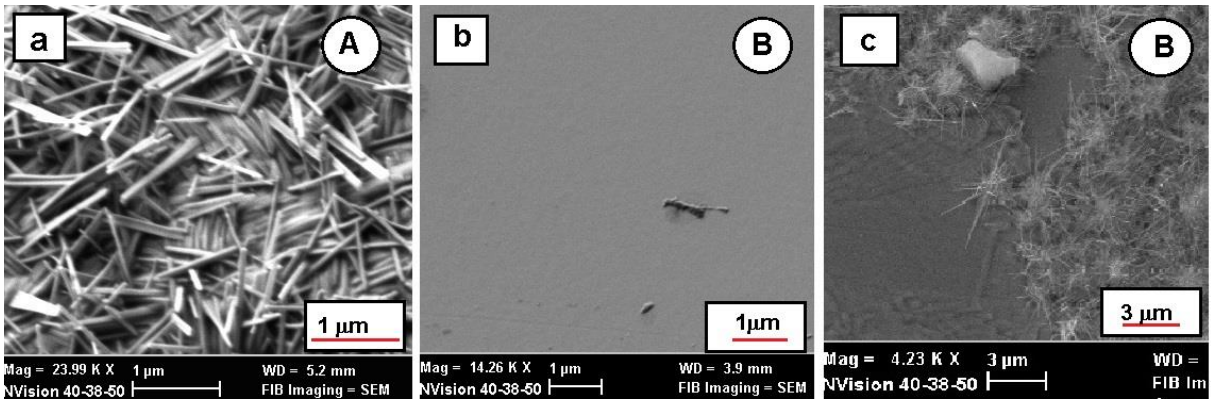

Figure 7. *The SEM images of frontal A-fracture (a) and lateral B-fracture (b, c) for Se (0%Te) sample observed after 1 month - SEM1 in Table 1 (a, b) and 3.5 months - SEM 2 (c) of storage.*

The anisotropy of microstructure (compare Fig. 7a and Fig. 7b) correlates with optical anisotropy observed for the same Se(0%Te) sample (compare spectra 12A and 12B in Fig. 5b), as well as with the transparency values in Table 1 for step 12. The latter means that the sample is three times more transparent in the lateral direction (B) than in the frontal direction (A): **T***(B)/**T***(A)=13.8/4.18=3.3 (see the directions of optical measurement in Fig. 2d). The relation **T***(B)>>**T***(A) seems reasonable because A-fracture contains ScO in the form of needles (Fig. 7a), while B-fracture is empty (Fig. 7b). The problem is not only in the fact that SEM relates to the local volume of the sample while the spectrum 12 relates to the whole sample including surface ScO, but also in different moments of measuring (just after the last US-treatment for optical transmission and after 1 month for SEM). As shown in Fig. 7c, after 2.5 months the needles appear on the lateral fracture too. Therefore, one can conclude only that the growth rate of the needle development is anisotropic.

The same relation between optical and SEM anisotropies is true for the “extremal” 2%Te sample: $\mathbf{T^*_A}$(1.5%)>>$\mathbf{T^*_B}$(0.4%), and accordingly, lateral B-fracture is much more distorted than frontal A-fracture in Fig. 8. Note, however, the **inversion of anisotropy**: **T***(A)/**T***(B)=3.8.

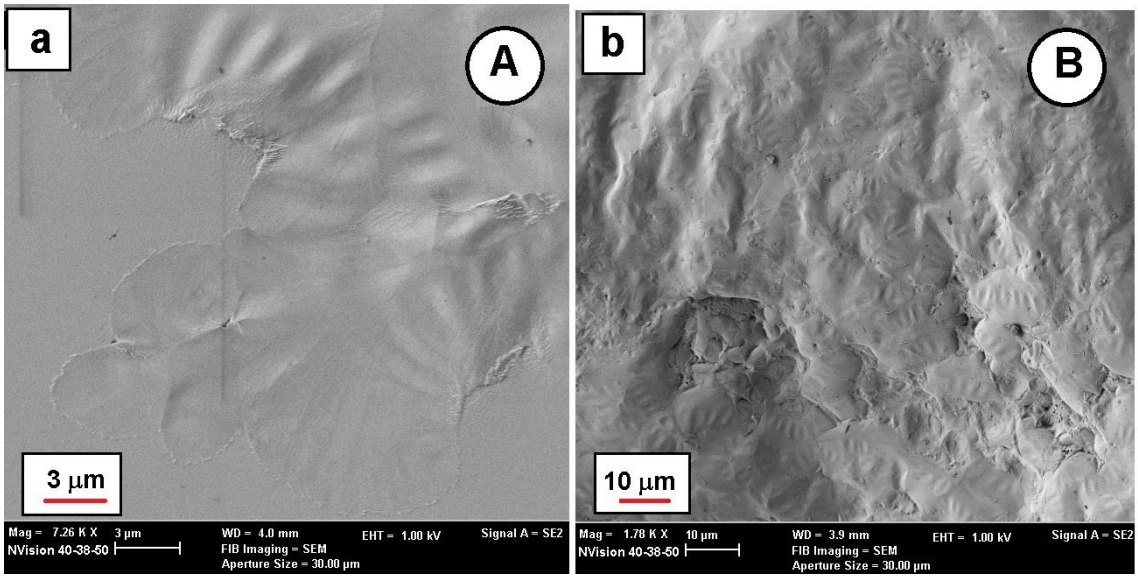

Figure 8. *SEM images of frontal (a) and lateral (b) fractures of Se-2%Te after the 1-month storage.*

Remember that “extremal” 2%Te composition corresponds to maximum nonlinearity of the concentration-property dependences, e.g., of the **G**=f(%Te) dependence in Fig. 4a for Se-Te. The SEM images of other “extremal” samples in Se-X series are shown in Fig. 9.

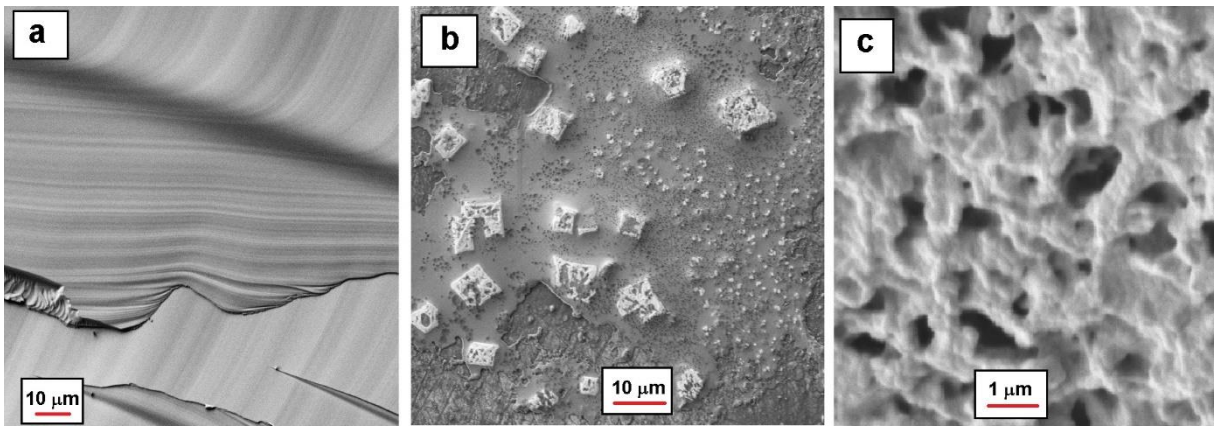

Figure 9. *SEM images for fractures of Se glass containing 0.25%As (a), 1%S (b) and 0.05%Cl (c).*

4. Discussion

The most striking facts presented in Section 3 are: (1) A strong acceleration of crystallization by means of cavitation treatment of softening glass - minutes vs years for the spontaneous crystallization for a similar transparency effect (compare **T*** for steps ‘U1” and “R1” in Table 1); (2) A high sensitivity of the optical transmission method for detection of early stage of crystallization (Figs. 3, 5); (3) Optical heterogeneity evaluated by mechanical resection of the surface layer (Fig. 4a); (4) Unusual microstructure of the treated samples revealed by SEM fractography (Figs. 7, 8, 9); (5) The cavitation-induced anisotropy (Figs. 5, 7, 8); (6) Nonlinearity induced by small addition of foreign atoms (Figs. 4, 7, 8, 9). The bond wave model presented in Section 2 (Figs. 1, 2) permits to interpret them on a unified basis as follows.

(1) The cavitation-induced acceleration of the crystallization process is a well-known phenomenon observed in various materials (e.g., [28], [29]) - but not in glass, where ultrasonic treatment was restricted so far to a simple smoothing of the glass surface [30]. According to the bond wave model, 3D bond waves need to be reconstructed not only the surface but also the volume, a condition that demands to rise temperature at least up to the softening state existing few tenths degrees above T_g, which is about 35ºC. To ensure that just cavitation, and not temperature alone, is the primary cause of the observed acceleration, a fresh Se sample of the same form was immersed into the cell filled with hot water at 72ºC for 5 minutes. There was no difference in the transmission spectra measured before and after the treatment. Thus, the main function of elevated temperature is to provide mobile 3D bond waves for effective action of cavitation field on the sample volume in accord with Fig. 2d, where ultrasonic field acts as the information field [31] that directs the waves (Fig. 1b). Of course, temperature also assists in intensifying the waves themselves (see [12] for details), which is demonstrated by an increasing effect of cavitation treatment when passing from the low-temperature (40-50ºC) treatments to the higher temperature (72ºC) final treatment (see **T*** values in Table 1).

(2) Since the final samples appeared glassy to the naked eye, no appreciable crystalline phase had developed by the end of the experiment, when the samples became almost opaque by optical transmission. Thus, the observed change in transmission (Figs. 3, 4, 5) relates to the early stage of crystallization which connects probably to the pre-nucleation phenomena, which are studied intensively in polymers [32] but not in inorganic glasses. Although optical transmission is sensitive to (pre)nucleation, it gives a restricted information, and there is the need of other methods such as SEM, SAXS, STEM-HAADF [33], etc. to characterize the size and morphology of the corresponding scattering objects.

(3) The tendency of glass for surface crystallization is a well-known property. The unexpected result is the non-linear influence of small additions on the optical heterogeneity, considered as a surface/volume distribution of the scattering objects. It is demonstrated in Fig. 4a for the simplest Se-Te system, in which one can see a jump from almost completely heterogeneous 0%Te sample to almost completely homogeneous 2%Te sample. This non-linearity not only emphasizes the self-organization nature of glass but also underscores the role of the glass surface as a scene for specific interaction between internal 3D bond waves and external medium.

(4) Since glass fracture runs along the wavefronts [23] as the layers enriched in relatively weak alternative bonds (see layers ‘1’ in Fig. 1a), SEM visualizes the wavefront microstructure that has developed before the survey. Unexpectedly, one observes no isolated nuclei but the extended textures such as the carpet of needles (Fig. 7a), “clouds” (Fig. 8), intersected waves (Fig. 9a) and “sponge” (Fig. 9c). The special cases of the “spider attack” (Fig. 7c) to the initially empty wavefront (Fig. 7b) for Se, as well as of two families of crystallites in Fig. 9b for Se-1%S, correspond to the later stage of crystallization. Then the process of crystallization can be divided into three steps: (i) activation - the pre-crystalline ordering of chemical bonds within the moving (at $T>T_g$) or stopped (at $T<T_g$) wavefronts; (ii) the 2D crystallization of the stopped wavefronts in solid glass ($T<T_g$), a process that is accompanied by the expulsion of alternative bonds on the wavefront boundaries; (iii) the 3D crystallization at $T<T_g$ when alternative bonds migrate from the wavefront into the surrounding network (Fig. 2a,b), thus ensuring the volume crystallization, or crystal growth, in solid glass. Note that steps (i) and (ii) are provided by the 2D bond waves which spreads along the wavefronts both above and below T_g [11], [12], while step (iii) proceeds only in solid glass. The high-temperature crystallization ($T>>T_g$) is a special process (see, e.g., Fig. 2c) which will be considered elsewhere.

(5) The anisotropy observed by optical transmission (Fig. 5) and by in SEM images (Figs. 7, 8) is a consequence of the anisotropic information field acting during cavitation treatment (see Fig. 2d).

(6) Interestingly, the concentration-property *nonlinearity* has been observed in fresh Se-X glasses by ultrasound velocity and X-ray fluorescence (Fig. 5 in [24]) but not by transparency (**T***=66±2% for all fresh samples). Non-linear behavior becomes apparent only after crystallization begins. Therefore, optical transmission is sensitive to the pre-crystallization ordering of the wavefronts but not to the initial wavefronts which remain transparent in the absence of (pre)crystalline formations. Regarding the nature of this nonlinearity, one can suppose that embedding X atoms can act either in a classical way by forming a mixed "topological" network, or, in a non-classic way, when the network recognizes them as foreign agents and produces a strong collective response. The open questions are why this reaction occurs at a definite "extremal" concentration and what are the mechanisms of this recognition and response.

The proposed model of crystallization seems not so strange if one recognizes bond wave as a natural source of intrinsic heterogeneity, a concept that is widely debated now (e.g., [33], [34]). It is proposed, in particular, that crystallization proceeds in "soft" (liquid-like) regions of non-crystalline structure but not in the "rigid" (solid-like) ones [35]. The liquid-like regions can be compared with the wavefronts ('1' in Fig. 1a) which, being populated with high-energy alternative bonds, represent the sites for collective rearrangement of basic/covalent bonds during bond switching events: $AB+CB_{1\text{-}2} \rightarrow CB_{2\text{-}3}+AB$, etc. The wavefronts can also be compared with the Cooperatively Rearranging Regions (CRR) after Adam and Gibbs [36]. Note that the concept of alternative bonds in the form of "soft" hypervalent bonds (HVB) was intensively developed by Dembovsky from both phenomenological and quantum-chemical points of views (see [21] for first publication and [22] for review). Only multicentre HVB (e.g., three-centre bonds in Fig. 1a) provides the low-energy non-breaking mechanisms for covalent bond switching from some atoms to others. Bond waves ensure the collective switching of basic bonds, a necessary condition for macroscopic processes such as viscous flow and crystallization.

Finally, the combination of cavitation treatment and the bond wave approach may be applied in practice in fields involving crystallization such as the preparation of glass-ceramics [37] or components for microelectronics [38]. The arising technological problems, e.g., those concerning cavitation medium for ceramics (water has a too low boiling point for most ceramic compositions) are compensated by the ability to produce anisotropic materials with unusual microstructures.

5. Conclusions

The experiments of accelerated crystallization by means of cavitation treatment of softening glass, considered through the eyes of the bond wave mode, permit to understand the enormously large lag time for nucleation as the time needed for a suitable reconstruction of the 3D bond wave wavefronts. Ultrasonic field, when interacting with softening glass, decreases the time for the "initial reorientation" of chemical bonds within the wavefronts, a reconstruction necessary to start crystallization process. The proposed non-classical model for nucleation treats the wavefronts as extended 2D "nuclei", naturally present in glass, which wait for activation/reconstruction to form "critical nuclei". This contrasts with microscopic 3D crystal-like formations which wait for reaching a critical size to be ready for the following continuous growth in classical nucleation theory (CNT). A basic difference is the well-ordered formation of these 2D nuclei - instead of random appearance of classical 3D nuclei by means of accidental "thermal fluctuations" in CNT. Then the "intrinsic inhomogeneities", both structural and dynamical, and "cooperatively rearranging regions" acquire a real form as wavefronts which can be observed in specific experiments. The general conclusion is justification of the self-organization nature of the glassy state which, therefore, deserves a greater attention in both glass science and glass technology, including a reasonable usage of specific methods developed for other self-organizing systems.

Acknowledgements

The author thanks G. E. Snopatin, V. S. Shiryaev and M. F. Churbanov for preparation of high-purity Se-X samples, E. V. Kisterev for US-treatments, E. B. Kryukova for measurement of the optical transmission spectra, and Russian Foundation of Basic Research (grant Nos. 05-03-33047 and 09-03-01158) for financial support. A special gratitude to S. A. Dembovsky (1932-2010) for the years of scientific co-working and support.

References

[1] J. C. Dyre., "*Colloquium*: The glass transition and elastic models of glass-forming liquids", Rev. Mod. Phys., vol. 78, pp. 953-972, 2006, doi: 10.1103/RevModPhys.78.953.
[2] D. Turnbull and M. H. Cohen, "Concerning reconstructive transformation and formation of glass", J. Chem. Phys., vol. 29, pp. 1049-1054, 1958, doi: 10.1063/1.1744654.
[3] M. C. Weinberg, D. R. Uhlmann and E. D. Zanotto, "Nose method of calculating critical cooling rates for glass formation", J. Amer. Ceram. Soc., vol. 72, pp. 2054-2058, 1989, doi: 10.1111/j.1151-2916.1989.tb06030.x.
[4] S. Krüger and J. Deubener, "Lag time to crystal nucleation of supercooled lithium disilicate melts: A test of the classical nucleation theory", J. Non-Cryst. Sol., vol. 426, pp. 1-6, 2015, doi: 10.1016/j.jnoncrysol.2015.06.023.
[5] S. A. Dembovsky and E. A. Chechetkina, "Kinetico-themodynamic aspect of glass formation and critical cooling rates in chalcogenide systems", Mater. Res. Bull., vol. 16, pp. 505-511, 1981, doi: 10.1016/0025-5408(81)90115-X.
[6] W. H. Zachariasen, "The atomic arrangement in glass", J. Amer. Chem. Soc., vol. 54, pp. 3841-3851, 1932, doi: 10.1021/ja01349a006.
[7] J. C. Mauro. "Topological constraint theory of glass", Amer. Ceram. Soc. Bull., vol. 90, pp. 31-35, 2011.
[8] P. Boolchand, G. Lucovsky, J. C. Phillips and M. F. Thorpe. "Self-organization and the physics of glassy networks", Philos. Mag., vol. 85, pp. 3823-3838, 2005, doi: 10.1080/14786430500256425.
[9] H. Haken. "Synergetics. An Introduction" (3rd ed.), Springer, Berlin-Heidelberg, 1983.
[10] R. Feistel and W. Ebeling. "Physics of Self-Organization and Evolution", Wiley-VCH, Berlin, 556 pp., 2011.
[11] E. A. Chechetkina, "Self-organization in glass: The synergetic chemical bonding approach", J. Optoel. Adv. Mater., vol. 18, pp. 44-49, 2016.
[12] E. A. Chechetkina, "Glass clarified as the self-organizing system", arXiv, 2024, doi: 10.48550/arXiv.2405.00346.
[13] E. A. Chechetkina, "Viscous flow in glass-forming liquids: The twice activation analysis and the bond wave mode", arXiv, 2025, doi:10.48550/arXiv.2509.11211.
[14] E. A. Chechetkina, E. V. Kisterev, E. B. Kryukova and A. I. Vargunin, "Crystallization of Se-As glasses in ultrasonic field according to optical transmission data", Inorg. Mater.: Appl. Res., vol. 2, pp. 360-369, 2011, doi: 10.1134/S2075113311040046.
[15] E. A. Chechetkina, E. V. Kisterev, E. B. Kryukova, A. I. Vargunin and S. A. Dembovsky, "Preparation of chalcogenide glass-ceramic materials by ultrasonic treatment of glasses", Inorg. Mater.: Appl. Res., vol. 3, pp. 11-17, 2012, doi: 10.1134/S2075113312010030.
[16] A. A. Vaipolin and E. A. Porai-Koshits, "X-ray study of glassy arsenic chalcogenides", Fiz. Tverd. Tela (Russ. Solid State Phyz.), vol. 5, pp. 246-255, 1963.
[17] S. R. Elliott, "Medium-range structural order in covalent amorphous solids", Nature, vol. 354, pp. 445-452, 1991, doi: 10.1038/354445a0.
[18] C. Massobrio and A. Pasquarello, "Origin of the first sharp diffraction peak in the structure factor of disordered network-forming systems: Layers or voids?", J. Chem. Phys., vol. 114, pp. 7976-7979, 2001, doi: 10.1063/1.1365108.

[19] E. A. Chechetkina, “Rawson’s criterion and intermolecular interactions in glass-forming melts”, J. Non-Cryst. Sol. vol. 128, pp. 30-47, 1991, doi: 10.1016/0022-3093(91)90774-z.
[20] E. A. Chechetkina, “Medium-range order in amorphous substances: A modified layer model”, Solid State Commun., vol. 91, pp. 101-104, 1994, doi: 10.1016/0038-1098(94)90262-3.
[21] S. A. Dembovsky, “Connection of quasidefects with glass formation in the substances with high lone-pair concentration”, Mater. Res. Bull., vol. 16, pp. 1331-1338, 1981, doi: 10.1016/0025-5408(81)90105-7.
[22] S. A. Dembovsky and E. A. Chechetkina, “Glassy materials clarified through the eyes of hypervalent bonding configurations”, J. Optoel. Adv. Mater., vol. 3, pp. 3-18, 2001.
[23] E. A. Chechetkina, “Fracture and fractals in glasses”, MRS Proc., vol. 367, pp. 397-402, 1994, doi: 10.1557/proc-367-397.
[24] E. A. Chechetkina, “Crystallization in glass forming substances: The chemical bond approach”, In: Crystallization - Science and Technology (ed. M. R. D. Andreeta), InTech. pp.3-28, 2012, doi: 10.5772/50539.
[25] K. J. Siemsen and H. D. Riccius, “Multiphonon processes in amorphous selenium”, J. Phys. Chem. Sol., vol. 30, pp. 1897-1900, 1969, doi: 10.1016/0022-3697(69)90257-1.
[26] M. C. Assuncao, “Effect of halogen impurities on selenium glasses”, J. Non-Cryst. Sol., vol. 136, pp. 81-90, 1991, doi: 10.1016/0022-3093(91)90122-M.
[27] M. F. Churbanov, “Recent advances in preparation of high-purity chalcogenide glasses in the USSR”, J. Non-Cryst. Sol., vol. 140, pp. 324-330, 1992, doi: 10.1016/S0022-3093(05)80790-2.
[28] J. R. G. Sander, B. W. Zeiger and K. S. Suslick, “Sonocrystallization and sonofragmentation”, Ultrason. Sonochem., vol. 21, pp. 1908-1915, 2014, doi: 10.1016/ultrasonch.2014.02.005.
[29] N. S. Deora, N. N. Misra, A. Deswal, H. N. Mishra, P. J. Cullen and B. K. Tiwari, “Ultrasound for improved crystallization in food processing”, Food. Eng. Rev., vol. 5, pp. 36-44, 2013, doi: 10.1007/s12393-012-9061-0.
[30] B. S. Lunin and A. L. Nikolaev, “Effect of ultrasonic treatment on the surface topography of quartz glass”, Inorg. Mater., vol. 59, pp. 306-310, 2023, doi: 10.1134/S0020168523030093.
[31] H. Haken and J. Portugali, “Information and self-organization: A unifying approach and applications”, Entropy, vol. 18, 197, pp. 1-57, 2016, doi: 10.3390/e18060197.
[32] A. Wurm, R. Soliman, J. G. P. Goossens, W. Bras, and C. Schick, “Evidence of precrystalline order in supercooled polymer melt revealed from simultaneous dielectric spectroscopy and SAXS”, J. Non-Cryst. Sol., vol. 351, pp. 2773-2779, 2005, doi: 10.1016/j.jnoncrysol.2005.04.072.
[33] L. Cormier, “Nucleation in glasses - new experimental findings and recent theories”, Pro. Mater. Sci., vol. 7, pp. 60-71, 2014, doi: 10.1016/ j.mspro.2014.10.009.
[34] H. Tanaka, “Structural origin on dynamic heterogeneity in supercooled liquid”, J. Phys. Chem. B, vol. 129, pp. 789-813, 2025, doi: 10.1021/acs.jpcb.4c06392.
[35] A. S. Abysov, V. M. Fokin, N. S. Yuritsyn, A. M. Rodrigues and J. W. P. Schmeltzer, “The effect of heterogeneous structure of glass-forming liquids on crystal nucleation”, J. Non-Cryst. Sol., vol.462, pp. 32-40, 2017, doi: 10.1016/j.jnoncrysol.2017.02.004.
[36] G. Adam and J. H. Gibbs, On the temperature dependence of cooperative relaxation properties in glass-forming liquids”, J. Chem. Phys., vol. 43, pp. 139-146, 1965, doi: 10.1063/1.1696442.
[37] C. Russel and W. Wisniewski, “Glass-ceramic engineering: tailoring the microstructure and properties”, Prog. Mater. Sci., vol. 152, 101437, pp. 1-71, 2025, doi: 10.1016/j.pmatsci.2025.101437.
[38] E. A. Chechetkina, “Photostructural changes and electrical switching in amorphous chalcogenides: Bond waves in thin films”, Nat. Sci., vol. 10, pp. 70-80, 2018, doi: 10.4236/ns.2018.102007.